Journal of Fluids and Structures (2002) **16**(8), 1029–1049
doi:10.1006/jfls.2002.0457 available online at http://www.idealibrary.com on IDEAL®

WAVE PROPAGATION IN A SYSTEM OF COAXIAL TUBES FILLED WITH INCOMPRESSIBLE MEDIA: A MODEL OF PULSE TRANSMISSION IN THE INTRACRANIAL ARTERIES

S. Cirovic

Institute for Aerospace Studies, University of Toronto, 4925 Dufferin Street Toronto, Ontario, Canada, M3H 5T6

C. Walsh
Flat Water Solutions Inc., 141 Maplewood Ave., Toronto, Ontario, Canada M6C IJ8

AND

W. D. Fraser
Defence and Civil Institute of Environmental Medicine, P.O. Box 2000 Toronto, Ontario, Canada, M3M 3B9

(Received 5 October 1999; and in final form 21 November 2001)

The propagation of harmonic waves through a system formed of coaxial tubes filled with incompressible continua is considered as a model of arterial pulse propagation in the craniospinal cavity. The inner tube represents a blood vessel and is modelled as a thin-walled membrane shell. The outer tube is assumed to be rigid to account for the constraint imposed on the vessels by the skull and the vertebrae. We consider two models: in the first model the annulus between the tubes is filled with fluid; in the second model the annulus is filled with a viscoelastic solid separated from the tubes by thin layers of fluid. In both models, the elastic tube is filled with fluid. The motion of the fluid is described by the linearized form of the Navier–Stokes equations, and the motion of the solid by classical elasticity theory. The results show that the wave speed in the system is lower than that for a fluid-filled elastic tube free of any constraint. This is due to the stresses generated to satisfy the condition that the volume in the system has to be conserved. However, the effect of the constraint weakens as the radius of the outer tube is increased, and it should be insignificant for the typical physiological parameter range.

1. INTRODUCTION

Analytic models of wave propagation in fluid-filled elastic tubes have been used extensively to describe pulse propagation in the arterial system (Lamb 1898; Womersley 1955; Cox 1968). The most compact analysis to date was given by Womersley (1955), who obtained a simple closed-form solution for the long wave speed in a freely moving thin-walled tube filled with a viscous fluid. Numerous attempts have been made since to

0889-9746/02/081029 + 21 $35.00/0

upgrade the theory of arterial blood flow and pressure propagation. Much of the effort has been focused on vessel modelling, either to introduce a thick-walled approximation for the tube (Cox 1968), or to include features such as initial stress and anisotropy (Atabek & Lew 1966; Atabek 1968). More recently, the emphasis has been on introducing the nonlinear fluid terms into analysis (Ling & Atabek 1972; Wang & Tarbell 1992). This type of modelling, however, typically requires a numerical solution. Linear pulse propagation models can be divided into freely moving and constrained, with respect to whether the interaction of the tube with the surrounding tissue is ignored or not (Cox 1969). Constrained models vary in complexity, from those which simply assume that the longitudinal motion is zero (Ling & Atabek 1972), to those which approximate the surrounding tissue as an additional mass (Womersley 1957*a*), or a mass, spring, dashpot system (Atabek 1968). Dinar (1975) treated the surrounding tissue as infinite viscoelastic continuum and concluded that the wave speed is affected mainly by the viscosity of the surrounding structures.

We are interested in pulse propagation in the craniospinal cavity; the craniospinal cavity is confined by the skull and vertebrae, and filled by the nervous tissue, blood vessels, and cerebrospinal fluid (CSF), which are all largely comprised of water, and are thus essentially incompressible (Ruan *et al.* 1991). Since the skull and vertebrae are effectively rigid, it is routinely assumed that the total cranial volume does not change. This is expressed through the Monroe–Kelly principle, which states that the sum of the blood, CSF, and tissue volume inside of the craniospinal cavity must always stay constant (Ursino 1988). The total volume of the cavity is 1 600–1 700 cm^3; about 150 cm^3 of that volume is occupied by the CSF, 100 cm^3 by blood, and the remainder by the brain and the spinal cord (Takemae *et al.* 1987; Guyton & Hall 1996). Most of the CSF is contained within the ventricles of the brain. The CSF also occupies the space between pia mater and arachnoid membrane of the brain and spinal cord (subarachnoid space), the space between the arachnoid membrane and dura (epidural space), and the space between the blood vessels and the nervous tissue (perivascular space) (Gray 1948). There is strong evidence of interaction between blood flow and CSF dynamics; there is a CSF pulse, which is a reflection of the blood pressure pulse (Lakin & Gross 1992; Portnoy & Chopp 1994); pathologically raised CSF pressure is associated with a drop in the cerebral blood flow and increase in the pulsatility of the CSF pressure (Kety *et al.* 1947); there is a significant pulsatile movement of the CSF in the spinal cavity (Loth *et al.* 2001).

Our goal is to develop a linear model of pulse propagation that will take account of the conservation of volume in the craniospinal cavity. In order that conservation of volume be imposed, the transverse dimension of the system representing cranial circulation has to be finite. Also, all of the intracranial components (blood, nervous tissue, CSF) have to be represented in the model, and treated as continua. The focus is on identifying the effect of the skull (vertebrae) constraint on pulse propagation. Therefore, we choose a simple model for the vessel wall, that will allow us to directly evaluate the effect of the constraint by comparing the results of the model with well-established solutions provided by Lamb (1898) and Womersley (1955).

2. METHODS

2.1. Model

We consider wave propagation in a system formed of coaxial circular tubes of infinite length. It is assumed that the wave amplitude is small so that the governing equations can

be linearized. The analysis is restricted to harmonic travelling waves of arbitrary wavelength. The inner tube, which represents a blood vessel, is flexible, while the outer tube, which represents the skull or vertebrae, is rigid. Both the flexible tube and the annulus between the tubes are filled with incompressible continua, representing blood, CSF, and nervous tissue. Therefore, the net volume flux through any cross-section of the model must be zero.

We examine two models that differ with respect to the content of the annulus between the tubes. In Model 1, all of the annulus is filled with fluid representing the CSF (Model 1 in Figure 1). Although this model is not very realistic, as it ignores the presence of the nervous tissue, it is useful for obtaining an immediate insight into the effect of the constraint on the pulse speed. In Model 2, the annulus is occupied by a viscoelastic solid, representing the nervous tissue, separated from both tubes by layers of viscous fluid, representing the CSF (Model 2 in Figure 1). The fluid layer between the rigid tube and the solid ($y_{c2} < y < y_0$, in Figure 1) represents the subarachnoid space, whereas the layer between the flexible tube and the solid ($1 < y < y_{c1}$, in Figure 1) represents the perivascular space. Both in Models 1 and 2 the flexible tube is occupied by fluid representing blood. For Model 1, we examine both the case where the fluids in the tube and the annulus are inviscid, and the case where the fluids are viscous. For Model 2, we consider only viscous fluids.

2.2. Governing Equations and Boundary Conditions

Wave propagation in the system considered involves the interaction between the vessel, the fluid contained within the vessel, and the contents of the annulus. Therefore, the

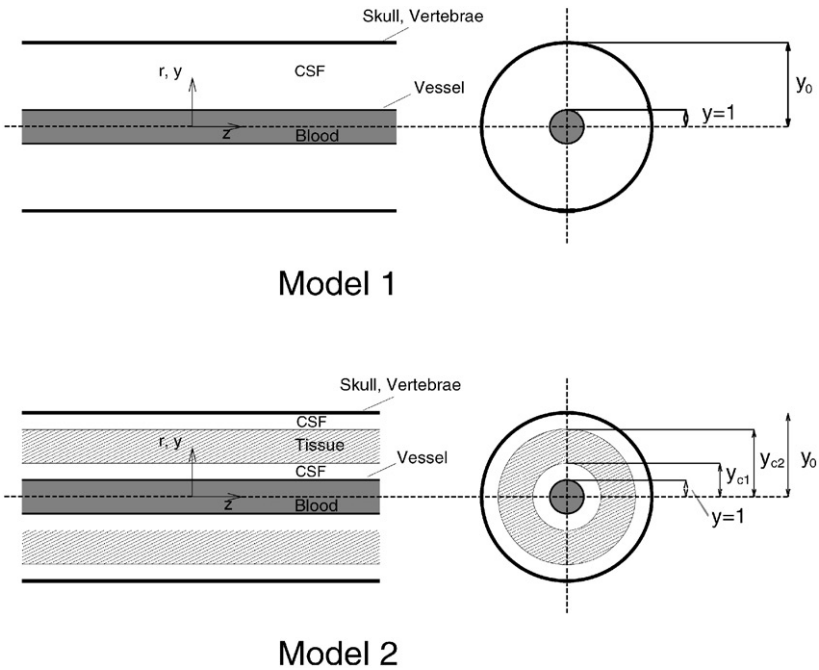

Figure 1. Models used in the analysis: An elastic tube (blood vessel) filled with incompressible fluid (blood) is enclosed within a rigid tube (skull, vertebrae). The annulus between the tubes is filled with incompressible continua. Model 1: The annulus between the tubes is filled with fluid (CSF). Model 2: The annulus between the tubes is filled with a viscoelastic solid (nervous tissue) separated from the tubes by fluid (CSF) layers of thickness $y_{c1} - 1$ (perivascular space) and $y_0 - y_{c2}$ (subarachnoid space).

mathematical statement of the problem involves the equations governing the motion of the vessel, fluid, and solid, as well as the boundary conditions at all of the interfaces. Since we are interested in small amplitude wave propagation, the governing equations and boundary conditions are given in their linearized forms.

2.2.1. Equations of motion of the vessel

We consider a thin cylindrical tube of undisturbed radius R and wall thickness h. The tube wall is homogeneous, isotropic, and linearly elastic, with Young's modulus E, density ρ, and Poisson's coefficient ε. The tube is subjected to action of radial and axial external force per unit area τ_r and τ_z. The equations of motion are

$$\begin{aligned}\frac{\partial^2\zeta}{\partial t^2} &= \frac{\tau_z}{\rho h} + \frac{E}{\rho(1-\varepsilon^2)}\left(\frac{\partial^2\zeta}{\partial z^2} + \frac{\varepsilon\,\partial\eta}{R\partial z}\right),\\ \frac{\partial^2\eta}{\partial t^2} &= \frac{\tau_r}{\rho h} - \frac{E}{\rho(1-\varepsilon^2)}\left(\frac{\varepsilon\,\partial\zeta}{R\partial z} + \frac{\eta}{R^2}\right),\end{aligned} \tag{1}$$

(Morgan & Kiely 1954; Womersley 1957*b*), where t is the time, z is the axial coordinate, and $\zeta(z,t)$ and $\eta(z,t)$ are axial and radial displacements of the tube wall, respectively.

2.2.2. Equations of motion of the fluid

We assume that blood and CSF are incompressible Newtonian fluids. We further assume that the flow is axially symmetric, body forces are absent, and the magnitudes of the velocity components and their derivatives are so small that their products can be neglected. Under these assumptions the Navier–Stokes and continuity equations in cylindrical coordinates reduce to

$$\begin{aligned}\frac{\partial v_z}{\partial t} &= -\frac{1}{\rho_f}\frac{\partial p}{\partial z} + \nu\left(\frac{\partial^2 v_z}{\partial z^2} + \frac{1}{r}\frac{\partial v_z}{\partial r} + \frac{\partial^2 v_z}{\partial r^2}\right),\\ \frac{\partial v_r}{\partial t} &= -\frac{1}{\rho_f}\frac{\partial p}{\partial r} + \nu\left(\frac{\partial^2 v_r}{\partial r^2} + \frac{1}{r}\frac{\partial v_r}{\partial r} - \frac{v_r}{r^2} + \frac{\partial^2 v_r}{\partial z^2}\right),\\ \frac{\partial v_z}{\partial z} &+ \frac{\partial v_r}{\partial r} + \frac{v_r}{r} = 0,\end{aligned} \tag{2}$$

where r is the radial coordinate, ρ_f is the density of the fluid, ν is the kinematic viscosity, p is the pressure, and v_z and v_r axial and radial components of velocity, respectively. The stresses in the fluid are

$$\sigma_{rr} = p - 2\mu\,\frac{\partial v_r}{\partial r}, \qquad \sigma_{rz} = \mu\left(\frac{\partial v_r}{\partial z} + \frac{\partial v_z}{\partial r}\right), \tag{3}$$

where μ is the dynamic viscosity of the fluid.

2.2.3. Equations of motion of the solid

The brain tissue is assumed to be linear, viscoelastic, isotropic and incompressible. The equations of motion and the condition of incompressibility in cylindrical

coordinates are

$$\begin{aligned}
\frac{\partial^2 u_z}{\partial t^2} &= -\frac{1}{\rho_s}\frac{\partial \Pi}{\partial z} + \frac{G}{\rho_s}\left(\frac{\partial^2 u_z}{\partial z^2} + \frac{1}{r}\frac{\partial u_z}{\partial r} + \frac{\partial^2 u_z}{\partial r^2}\right),\\
\frac{\partial^2 u_r}{\partial t^2} &= -\frac{1}{\rho_s}\frac{\partial \Pi}{\partial r} + \frac{G}{\rho_s}\left(\frac{\partial^2 u_r}{\partial r^2} + \frac{1}{r}\frac{\partial u_r}{\partial r} - \frac{u_r}{r^2} + \frac{\partial^2 u_r}{\partial z^2}\right),\\
\frac{\partial u_z}{\partial z} &+ \frac{\partial u_r}{\partial r} + \frac{u_r}{r} = 0,
\end{aligned} \tag{4}$$

(Love 1944). Here, ρ_s is the density of the solid, G the complex shear modulus, Π a finite pressure, and u_z and u_r are the axial and radial components of displacement, respectively. The stresses in the solid are

$$\sigma_{rr} = \Pi - 2G\frac{\partial u_r}{\partial r}, \qquad \sigma_{rz} = G\left(\frac{\partial u_r}{\partial z} + \frac{\partial u_z}{\partial r}\right). \tag{5}$$

2.4.4. Boundary conditions

The following boundary conditions have to be satisfied for Model 1.

(i) The kinematic condition at the wall of the rigid outer tube. In the case where inviscid fluids are considered, slip parallel to the boundary is allowed. Thus,

$$\text{at } y = y_0 \quad \begin{cases} v_z = 0 & \text{(viscous fluid only)},\\ v_r = 0. \end{cases} \tag{6}$$

(ii) The kinematic conditions at the flexible tube wall, both for the fluid in the tube and for the fluid in the annulus. In the case where inviscid fluids are considered, slip parallel to the boundary is allowed. Thus,

$$\text{at } y = 1 \quad \begin{cases} v_z = \dfrac{\partial \xi}{\partial t} & \text{(viscous fluid only)},\\ v_r = \dfrac{\partial \eta}{\partial t}. \end{cases} \tag{7}$$

(iii) Symmetry at $y = 0$ for the fluid in the flexible tube, i.e.,

$$\text{at } y = 0 \quad \begin{cases} \dfrac{\partial v_z}{\partial r} = 0,\\ v_r = 0. \end{cases} \tag{8}$$

For inviscid fluid, this reduces to a single condition, and either of equations (8) can be used.

The boundary conditions above also apply to Model 2, which must also satisfy: (a) the kinematic conditions at the fluid–solid boundaries in the annulus,

$$\text{at } y = y_{c1} \quad \text{and } y = y_{c2} \quad \begin{cases} v_z = \dfrac{\partial u_z}{\partial t},\\ v_r = \dfrac{\partial u_r}{\partial t}; \end{cases} \tag{9}$$

(b) continuity of stresses at the fluid–solid boundaries in the annulus,

$$\text{at } y = y_{c1} \text{ and } y = y_{c2} \quad \begin{cases} p - 2\mu\dfrac{\partial v_r}{\partial r} = \Pi - 2G\dfrac{\partial u_r}{\partial r}, \\ \mu\left(\dfrac{\partial v_r}{\partial z} + \dfrac{\partial v_z}{\partial r}\right) = G\left(\dfrac{\partial u_r}{\partial z} + \dfrac{\partial u_z}{\partial r}\right). \end{cases} \tag{10}$$

The total number of boundary conditions for Model 1 is four if the fluids in the tube and the annulus are inviscid, and eight if they are viscous. For Model 2, the total number of boundary conditions is 16. The boundary conditions are linearized in the sense that they are applied at the undisturbed rather than at the actual boundaries. The error introduced by the linearization of the boundary condition is of the same order of magnitude as that due to linearization of fluid equations (Morgan & Kiely 1954).

2.3. Solution

We consider the propagation of waves which are harmonic in t and z. Therefore, any variable $q(r, z, t)$ in equations (2)–(5) is assumed to be of the form

$$\bar{q}(r)\ \mathrm{e}^{\mathrm{i}\omega(t-z/c)}, \tag{11}$$

where ω is the circular frequency and c is the wave speed. Under this assumption the solutions of equations (2) and (4) are

$$\begin{aligned} \bar{p}(y) &= A'_f \mathrm{J}_0(\kappa y) + A''_f \mathrm{Y}_0(\kappa y), \\ \bar{v}_z(y) &= D'_f \mathrm{J}_0(\beta y) + D''_f \mathrm{Y}_0(\beta y) + \left(\frac{1}{\rho_f c}\right)[A'_f \mathrm{J}_0(\kappa y) + A''_f \mathrm{Y}_0(\kappa y)], \\ \bar{v}_r(y) &= \left(\frac{\kappa}{\beta}\right)[D'_f \mathrm{J}_1(\beta y) + D''_f \mathrm{Y}_1(\beta y)] + \left(\frac{1}{\rho_f c}\right)[A'_f \mathrm{J}_1(\kappa y) + A''_f \mathrm{Y}_1(\kappa y)], \end{aligned} \tag{12}$$

and

$$\begin{aligned} \bar{\Pi}(y) &= A'_s \mathrm{J}_0(\kappa y) + A''_s \mathrm{Y}_0(\kappa y), \\ \bar{u}_z(y) &= \left(\frac{1}{\mathrm{i}\omega}\right)\left\{D'_s \mathrm{J}_0(\gamma y) + D''_s \mathrm{Y}_0(\gamma y) + \left(\frac{1}{\rho_s c}\right)[A'_s \mathrm{J}_0(\kappa y) + A''_s \mathrm{Y}_0(\kappa y)]\right\}, \\ \bar{u}_r(y) &= \left(\frac{1}{\mathrm{i}\omega}\right)\left\{\left(\frac{\kappa}{\gamma}\right)[D'_s \mathrm{J}_1(\gamma y) + D''_s \mathrm{Y}_1(\gamma y)] + \left(\frac{1}{\rho_s c}\right)[A'_s \mathrm{J}_1(\kappa y) + A''_s \mathrm{Y}_1(\kappa y)]\right\}, \end{aligned} \tag{13}$$

(Cox 1968). Where $y = r/R$, $\mathrm{J}_n, \mathrm{Y}_n$ $(n = 0, 1)$ are nth order Bessel functions of the first and second kind, respectively, and A', A'', D' and D'' are constants. Also, $\gamma = \left\{[\omega^2 R^2/(G/\rho_s)] + \kappa^2\right\}^{1/2}$, $\beta = \left(\alpha^2 \mathrm{i}^3 + \kappa^2\right)^{1/2}$, $\alpha = R\left(\omega/\nu\right)^{1/2}$ (the Womersley number), and $\kappa = \mathrm{i}R\omega/c$. The parameter κ is proportional to the ratio of the flexible tube radius and the wavelength (λ). For inviscid fluids, β is infinite, and the first two terms on the right-hand side of the expressions for velocities in equations (12) are zero. The expressions for stresses are obtained by substituting equations (12) and (13) into (3) and (5).

The vessel displacements are of the form

$$\zeta = M\mathrm{e}^{\mathrm{i}\omega(t-z/c)}, \qquad \eta = N\mathrm{e}^{\mathrm{i}\omega(t-z/c)}, \tag{14}$$

where M and N are the amplitudes of the axial and radial tube motion, respectively. The external forces acting on the vessel wall are fluid stresses at the vessel wall ($y = 1$), and can be written as

$$\tau_z = \{(\bar{\sigma}^a_{rz} - \bar{\sigma}^t_{rz})_{y=1}\}e^{i\omega(t-z/c)}, \qquad \tau_r = \{(\bar{\sigma}^t_{rr} - \bar{\sigma}^a_{rr})_{y=1}\}e^{i\omega(t-z/c)}, \tag{15}$$

where superscripts t and a denote fluids in the tube and the annulus, respectively. The equations of motion of the elastic tube can now be rewritten as

$$\begin{aligned} &\frac{\omega^2}{\kappa\delta}\left\{(\delta - X)\kappa M + \varepsilon X N + \frac{(\bar{\sigma}^a_{rz} - \bar{\sigma}^a_{rz})_{y=1}}{i\omega\rho^t_f c}\right\} = 0, \\ &-\frac{\omega^2}{\kappa^2\delta}\left\{\varepsilon X\ \kappa M - (\kappa^2\delta + X)N + \frac{\kappa(\bar{\sigma}^t_{rr} - \bar{\sigma}^a_{rr})_{y=1}}{i\omega\rho^t_f c}\right\} = 0, \end{aligned} \tag{16}$$

where $\delta = h\rho/R\rho^t_f$ and $X = E\delta/[c^2\rho(1-\varepsilon^2)]$.

2.3.1. Solution for Model 1

The linearized solution of equations (2) is incorporated into the boundary conditions given in equations (6)–(8). Together with the linearized equations of motion of the elastic tube [equation (16)], this yields a homogeneous system of algebraic equations, where the unknowns are the constants in the expressions for the fluid velocities and the amplitudes of the vessel motion. The dimension of the system is 6×6, when the fluids in the tube and the annulus are inviscid, and 10×10 when the fluids are viscous. Since the system is homogeneous, the unknown constants cannot be calculated independently but they can be interrelated (Cox 1968). Thus, the boundary conditions can be used to express all of the remaining constants in terms of the amplitudes of the vessel motion. Then, the system is reduced to the equations of the vessel motion, where the only unknowns are M and N. The analysis is simplified by the fact that the situation relevant for pulse propagation in the arteries is the one where $k \ll 1$ (Cox 1968). Furthermore, if a long wave approximation is used, i.e., if it is assumed that the wavelength is much larger than the transverse dimensions of the system ($y_0 R/\lambda \ll 1$), the following asymptotic expressions can be used:

$$\beta \simeq \alpha i^{3/2}, \qquad J_0(\kappa y) \simeq 1, \qquad J_1(\kappa y) \simeq \frac{1}{2}\kappa y, \qquad Y_1(\kappa y) \simeq \frac{2}{\pi}\left(\frac{1}{\kappa y}\right) \tag{17}$$

since $\kappa y \ll 1$ (Atabek & Lew 1966). Also, for a typical physiological parameter range, the terms which are of the order $(\kappa/\alpha)^2$ compared with the leading terms can be ignored (Womersley 1957*a*).

We first consider the simplest case, in which both the tube and the annulus are filled with inviscid fluid. When the long wave approximation is used, the following expressions are obtained for the velocities and stresses in the tube

$$\bar{v}^t_z = \frac{A^t}{\rho^t_f c}, \qquad \bar{v}^t_r = \frac{A^t\,\kappa}{\rho^t_f c 2}y, \qquad \bar{\sigma}^t_{rr} = \bar{p}^t = A^t, \qquad \bar{\sigma}^t_{rz} = 0, \tag{18}$$

and in the annulus

$$\bar{v}^a_z = \frac{A^a}{\rho^a_f c}, \qquad \bar{v}^a_r = \frac{A^a\,\kappa}{\rho^a_f c 2}\left(y - \frac{y_0^2}{y}\right), \qquad \bar{\sigma}^a_{rr} = \bar{p}^a = A^a, \qquad \bar{\sigma}^a_{rz} = 0, \tag{19}$$

where $A^t = A^{\prime t}_f$, $A^a = A^{\prime a}_f$. Recall that superscripts t and a are used to distinguish whether a parameter is associated with the fluid in the vessel or with the fluid in the annulus between

the vessel and the rigid tube. The conditions that $\bar{v}_r^a|_{y=y_0} = 0$ and $\bar{v}_r^t|_{y=0} = 0$ are used to eliminate the constants $A_f''^t$ and $A_f''^a$. Upon applying the condition that $\bar{v}_r^t = \bar{v}_r^a = \mathrm{i}\omega N$ at the vessel wall, we obtain

$$\frac{\kappa(\bar{\sigma}_{rr}^t - \bar{\sigma}_{rr}^a)_{y=1}}{\mathrm{i}\omega\rho_f^t c} = 2\left(1 + \frac{\rho_f^a}{\rho_f^t}\frac{1}{y_0^2 - 1}\right)N. \tag{20}$$

Equations (20) and (16) can be combined into the following homogeneous system:

$$\begin{bmatrix} \delta - X & \varepsilon X \\ \varepsilon X & -X + 2\left(1 + \dfrac{\rho_f^a}{\rho_f^t}\dfrac{1}{y_0^2 - 1}\right) \end{bmatrix} \begin{Bmatrix} \kappa M \\ N \end{Bmatrix} = \begin{Bmatrix} 0 \\ 0 \end{Bmatrix}. \tag{21}$$

For a nontrivial solution to exist, the determinant of the system has to be zero. Therefore, the following dispersion equation has to be satisfied:

$$X^2 - \frac{\delta + 2(1 + (\rho_f^a/\rho_f^t)(1/(y_0^2 - 1)))}{1 - \varepsilon^2}X + \frac{2\delta(1 + (\rho_f^a/\rho_f^t)(1/(y_0^2 - 1)))}{1 - \varepsilon^2} = 0. \tag{22}$$

The long wave solution, for the case when the fluids in the annulus and the tube are viscous, is somewhat cumbersome and it will be discussed only in general terms. For the detailed derivation the reader should refer to Appendix A. When the constants A_f', A_f'', D_f', and D_f'' are eliminated using the boundary conditions, the terms associated with the external forces in equations (16) can be written as

$$\begin{bmatrix} \dfrac{(\bar{\sigma}_{rz}^a - \bar{\sigma}_{rz}^t)_{y=1}}{\mathrm{i}\omega\rho_f^t c} \\ \dfrac{\kappa(\bar{\sigma}_{rr}^t - \bar{\sigma}_{rr}^a)_{y=1}}{\mathrm{i}\omega\rho_f^t c} \end{bmatrix} = \begin{bmatrix} \frac{1}{2}\Theta_{zz} - \Theta_{rz} \\ -\Theta_{rz} 2\Theta_{rr} \end{bmatrix} \begin{Bmatrix} \kappa M \\ N \end{Bmatrix}, \tag{23}$$

where Θ_{zz}, Θ_{rz}, and Θ_{rr} are nondimensional functions of y_0, ρ_f^a/ρ_f^t, α^t, and α^a which are given in Appendix A. The dispersion equation is

$$X^2 - \frac{\delta + \frac{1}{2}\Theta_{zz} - 2\varepsilon\Theta_{rz} + 2\Theta_{rr}}{1 - \varepsilon^2}X + \frac{\Theta_{zz}\Theta_{rr} + 2\delta\Theta_{rr} - \Theta_{rz}^2}{1 - \varepsilon^2} = 0. \tag{24}$$

When y_0 is large, equations (17) may no longer be accurate for the fluid in the annulus, even if $\kappa \ll 1$. To test the validity of long wave approximation, we compared it with a solution for arbitrary wavelength, obtained by an iterative method that will be described in the next paragraph.

2.3.2. Solution for Model 2

The linearized solution of equations (2) and (4) is incorporated into the boundary conditions given in equations (6)–(10). Together with equations (16), this yields a homogeneous system of 18 algebraic equations. We use the same approach as for Model 1, where the boundary conditions are used to eliminate all of the unknown constants except the amplitudes of the vessel motion. However, the shear modulus of the brain tissue is of the order 10^3–10^4 Pa (Fallenstein *et al.* 1969; Galford & McElhaney 1970; Shuck & Advani 1972), γ is of the same order as κ, and the terms of the order $(\kappa/\gamma)^2$ compared with the leading terms can no longer be ignored. Consequently, for this model it is not possible to obtain a closed-form solution even if a long wave approximation is used and there is no

benefit from using the asymptotic expressions given in equations (17). The solution is obtained iteratively in the following way:

(i) the values of the parameters y_0 and α^t are chosen as independent variables;
(ii) an initial guess for parameter κ is made from the long wave result of Model 1 for the same values of y_0 and α^t;
(iii) current values of the parameters β^t, β^a, and γ are calculated from the chosen value of α^t and the current value of κ;
(iv) the current values of κ, β^t, β^a, and γ are substituted into the boundary conditions and all of the remaining unknown constants are expressed in terms of the amplitudes of the vessel motion using classical methods of linear algebra (Wylie & Barrett 1982);
(v) the results of the previous step are incorporated into equations (16) in order to eliminate all of the constants except M and N, and X is calculated from the condition that the determinant of the system must be zero.
(vi) the new values of c and κ are determined from the calculated X.

The procedure is repeated until the values of κ from two successive iterations are sufficiently close.

3. RESULTS

3.1. Model 1

The results were obtained using a long wave approximation, and tested using the full equations solved by the iterative method described in the previous section. We found the solution obtained by the two methods to be in excellent agreement for the range of parameters used in the simulations.

When the tube and the annulus are occupied by inviscid fluids, the wave speeds obtained from equation (22) for $\delta \ll 1$ are

$$c_1 \simeq \sqrt{\frac{E\delta}{2\rho_f^t\left(1+\dfrac{\rho_f^a}{\rho_f^t}\dfrac{1}{y_0^2-1}\right)}}, \qquad c_2 \simeq \sqrt{\frac{E}{\rho(1-\varepsilon^2)}}. \tag{25}$$

The first mode is called Young's mode and represents pressure waves propagating in the fluid, while the second, Lamb's mode, represents waves travelling within the wall (Cox 1969). For comparison, the solution for an unconstrained tube filled with inviscid incompressible fluid is

$$c_{01} \simeq \sqrt{\frac{E\delta}{2\rho_f^t}}, \qquad c_{02} \simeq \sqrt{\frac{E}{\rho(1-\varepsilon^2)}}, \tag{26}$$

(Lamb 1898). Therefore, the wave speed for Young's mode (c_1) decreases due to the constraint, whereas the wave speed for Lamb's mode (c_2) is not affected by the constraint. Inspection of equations (16) and (21) shows that the inertia term in the transverse equation

of the vessel motion can be written as

$$2\left(1+\frac{\rho_f^a}{\rho_f^t}\frac{1}{y_0^2-1}\right)-\kappa^2\delta \simeq 2\left(1+\frac{\rho_f^a}{\rho_f^t}\frac{1}{y_0^2-1}\right), \tag{27}$$

where $-\kappa^2\delta$ is the radial inertia term of a completely free empty tube (Graff 1991) which is positive and real since κ is purely imaginary. For an unconstrained tube filled with inviscid fluid, the radial inertia term is $-\kappa^2\delta+2$. The term $2(\rho_f^a/\rho_f^t)[1/(y_0^2-1)]$ accounts for the effect of the fluid in the annulus, and it can be interpreted as increase of the effective radial inertia. This term tends to zero with increasing y_0, meaning that the effect of the constraint weakens as the radius of the rigid tube increases. Figure 2 shows that the rate at which c_1 approaches c_{01}, with increasing y_0, depends on the ratio of ρ_f^a to ρ_f^t. For physiological applications, the most relevant case is the one where $\rho_f^a=\rho_f^c$, $c_1/c_{01}=\left(1-y_0^{-2}\right)^{1/2}$, and wave speeds of constrained and unconstrained vessels differ by $<1\%$ for $y_0=10$.

Pressures and velocities in the annulus can be related to those in the elastic tube using equations (18) and (19) and the condition that $\bar{v}_r^a|_{y=1}=\bar{v}_r^t|_{y=1}$. The fact that neither the pressure nor the axial velocity vary over a cross-section facilitates the analysis. The ratio of velocities in the annulus and the tube is given by

$$\frac{\bar{v}_z^a}{\bar{v}_z^t}=-\left(\frac{1}{y_0^2-1}\right). \tag{28}$$

The fluid in the annulus moves in the direction opposite to that of the fluid in the tube with a velocity that is inversely proportional to y_0^2-1. It follows from equation (28) that the volumetric flow rates in the elastic tube and the annulus are of the same magnitude but of the opposite sign and that the net volumetric flow rate in each cross-section is always zero. The ratio of the pressures is ρ_f^a/ρ_f^t times that of the velocity ratio which reflects the fact that, unlike the volume flux, the mass flux is not zero unless $\rho_f^a=\rho_f^t$:

$$\frac{\bar{p}^a}{\bar{p}^t}=-\frac{\rho_f^a}{\rho_f^t}\left(\frac{1}{y_0^2-1}\right). \tag{29}$$

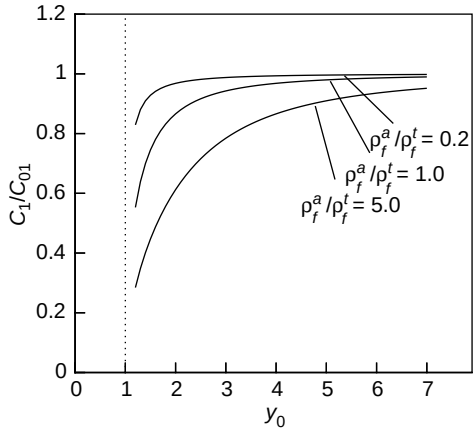

Figure 2. Wave speed for Young's mode in terms of parameter y_0, for Model 1 and inviscid fluids. The wave speed is normalized with respect to $c_{01}=(E\delta/2\rho_f^t)^{1/2}$.

It can be seen from equations (28) and (29) that $|\bar{v}_z^a| > |\bar{v}_z^t|$ for $y_0 < \sqrt{2}$, $|\bar{p}^a| > |\bar{p}^t|$ for $y_0 < (\rho_f^a/\rho_f^t + 1)^{1/2}$, and that both $\bar{v}_z^a$ and $\bar{p}^a$ rapidly decrease with increasing y_0. According to equations (18) and (19) the maximal radial velocity is at the vessel wall, both for the fluid in the tube and the fluid in the annulus. Therefore, the maximal values of the radial velocities in the tube and the annulus are the same regardless of y_0.

When the tube and the annulus are occupied by viscous fluids, the wave speed depends on α^t and α^a, as well as y_0, and ρ_f^a/ρ_f^t. We restricted the analysis to the values of parameters corresponding to the blood and CSF. Since the composition of the CSF is similar to that of blood plasma (Sullivan & Allison 1985), it was assumed that the density and viscosity of the CSF are the same as those of plasma and that $\mu^a/\mu^t = 0{\cdot}25$ and $\rho_f^a/\rho_f^t = 1$. It was also assumed that $\delta = 0{\cdot}1$. Then, the wave speed is a function of α^t and y_0 only. The phase speed and transmission per wavelength can be calculated from the complex wave speed obtained from equation (24). We show the results only for Young's mode since it is the mode relevant for blood pulse propagation. The phase speed and transmission per wavelength are shown as functions of α^t in Figures 3 and 4, and the results for three values of α^t and y_0 are tabulated in Table 1. The symbols indicate Womersley's solution for an unconstrained tube. In general, the effect of the constraint is to reduce the wave speed and increase the attenuation. This effect weakens with increasing y_0, and the solution approaches that of Womersley. For the parameters used in the study, the phase speed for the constrained tube differs by $< 5\%$ from that predicted by Womersley for $y_0 \geqslant 4$, whereas the effect of the constraint on the wave attenuation is weak for $y_0 \geqslant 2$. With increasing α^t, the inviscid solution is approached.

The velocity profiles can be reconstructed by assuming that the flow is driven by a harmonic pressure in the vessel, and expressing all of the remaining constants in terms of the pressure amplitude (A^t). Figure 5 displays velocity profiles over a half-cycle, for $y_0 = 1{\cdot}5$, and $\alpha^t = 2$ and 10. The velocity profiles are flatter for $\alpha^t = 10$ since the effect of viscosity becomes weaker at higher Womersley numbers. It is obvious from the figure that the bulk fluid motions in the tube and the annulus are in the opposite directions. The integration of the expressions for the axial velocity in the vessel and the annulus given in Appendix A yields the following results for the volumetric flow rates normalized with

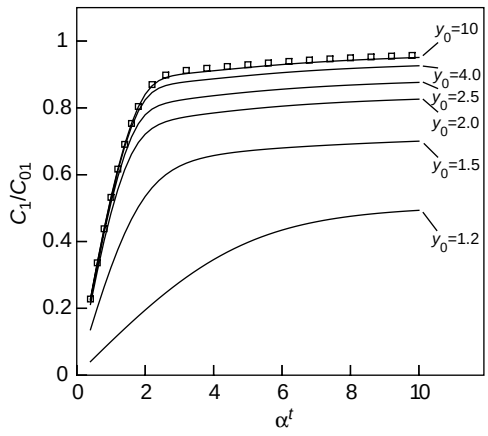

Figure 3. Phase velocity in terms of the Womersley number α^t, for Model 1 and viscous fluids. The phase velocity is normalized with respect to $c_{01} = (E\delta/2\rho_f^t)^{1/2}$. It was assumed that $\mu^a/\mu^t = 0{\cdot}25$, $\rho_f^a/\rho_f^t = 1$, and $\delta = 0{\cdot}1$. The solid lines show the solutions given by the model for different values of parameter y_0, and the symbols show Womersley's solution. The results are tabulated in Table 1.

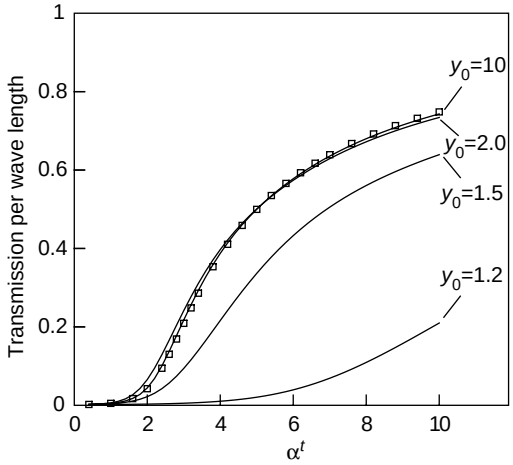

Figure 4. Transmission per wavelength in terms of the Womersley number α^t, for Model 1 and viscous fluids. It was assumed that $\mu^a/\mu^t = 0{\cdot}25$, $\rho_f^a/\rho_f^t = 1$, and $\delta = 0{\cdot}1$. The solid lines show the solutions given by the model for different values of parameter y_0, and the symbols show Womersley's solution. The results are tabulated in Table 1.

TABLE 1

Phase velocity and transmission per wavelength for Model 1 and viscous fluids, and Womersley's solution for the same values of α^t

			c_1/c_{01}	Trans. per λ
	Womersley		0·22789	0·00220
$\alpha^t = 0{\cdot}4$		$y_0 = 1{\cdot}5$	0·13609	0·00212
	Model 1	$y_0 = 2{\cdot}0$	0·21169	0·00231
		$y_0 = 4{\cdot}0$	0·22737	0·00222
	Womersley		0·84259	0·04238
$\alpha^t = 2{\cdot}0$		$y_0 = 1{\cdot}5$	0·53483	0·02194
	Model 1	$y_0 = 2{\cdot}0$	0·72117	0·06559
		$y_0 = 4{\cdot}0$	0·82404	0·05043
	Womersley		0·95769	0·74827
$\alpha^t = 10{\cdot}0$		$y_0 = 1{\cdot}5$	0·70032	0·63922
	Model 1	$y_0 = 2{\cdot}0$	0·82598	0·73409
		$y_0 = 4{\cdot}0$	0·92598	0·74756

respect to πR^2

$$2\int_0^1 \bar{v}_z^t y \, \mathrm{d}y = \frac{2}{\kappa}\bar{v}_r^t\Big|_{y=1},$$

$$2\int_1^{y0} \bar{v}_z^a y \, \mathrm{d}y = -\frac{2}{\kappa}\bar{v}_r^a\Big|_{y=1}. \tag{30}$$

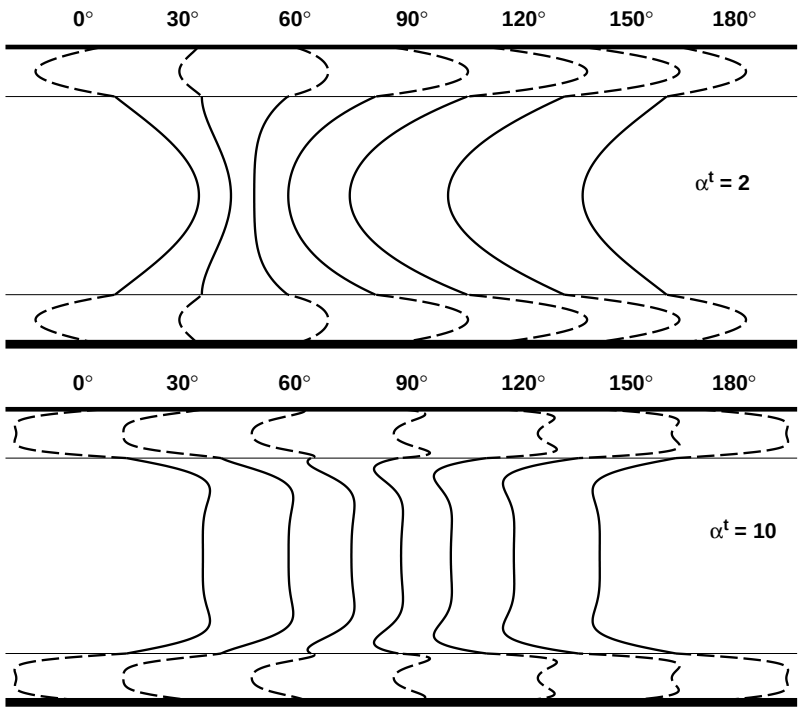

Figure 5. Velocity profiles over a half-cycle, for Model 1 and viscous fluids, calculated for $\alpha^t = 2$ (top) and $\alpha^t = 10$ (bottom). Solid line shows the profiles in the tube, while the broken line shows the profiles in the annulus. Bold line represents the rigid tube.

Since the kinematic condition at the tube wall requires that $\bar{v}_r^t|_{y=1} = \bar{v}_r^a|_{y=1}$, the volume fluxes in the tube and the annulus are of the same magnitude and of the opposite sign, and the volume conservation is satisfied.

3.2. Model 2

This relatively complex model introduces two new geometric parameters: y_{c1} and y_{c2}, as well as physical properties of the solid, which can strongly influence the solution. Moreover, by introducing another elastic structure in the model, we may expect that the dispersion equation has more than two roots, even for the long wave case. However, since we are mainly interested in blood pulse propagation, we restrict our attention to a physiologically plausible range of parameters and Young's mode of wave propagation. The brain tissue is modelled as a standard viscoelastic solid based on the experimental results reported by Shuck & Advani (1972). The vessel radius and elastic properties are chosen to represent larger cranial and spinal arteries and are based on the values reported by Hilen *et al*. (1986), Zagzoule & Marc-Vergnes (1986), and Sheng *et al*. (1995). Based on the typical diameter of the anterior spinal artery of approximately 1 mm (Dommisse 1975) and the typical width of the vertebral canal of approximately 10–20 mm (Lang 1993), the minimal value of the parameter y_0 for the spine is approximately 10. For the arteries in the cranium y_0 is larger, since the typical width of the skull is approximately 150 mm (Wismans & Van Oorschot 1993), whereas the radius of the largest intracranial arteries is approximately 2–3 mm. We choose $y_0 = 10$ as a physiologically plausible value that maximizes the effect of the constraint. The value of $y_{c2} = 8$ is based on the fact that the

subarachnoid space hosts some of the larger veins, such as the interior venous plexus in the spine. Unfortunately, there is little quantitative information in the literature about the dimensions of the perivascular space, which is present up to the level of microcirculation (Guyton & Hall 1996). Based on the qualitative observations, the width of the perivascular space should be of the order of magnitude of the vessel diameter (Gluhbegovic & Williams 1980). We therefore consider $y_{c1} = 1{\cdot}1$ and $2{\cdot}0$ as the extreme cases. The values of the parameters used in the simulations are summarized in Table 2.

The results are displayed in Figures 6 and 7 and tabulated in Table 3. We see from the figures that there is little difference between the predictions of the model and the Womersley solution for $y_{c1} = 2{\cdot}0$. It should be noted that replacing the standard

TABLE 2

The parameters used in the simulation involving Model 2

Geometry	y_{c1}	$2{\cdot}0$ or $1{\cdot}1$
	y_{c2}	$8{\cdot}0$
	y_0	$10{\cdot}0$
Flexible tube	R	10^{-3} m
	h	10^{-4} m
	ρ	10^3 kg m^3
	E	4×10^6 Pa
	ε	$0{\cdot}5$
Fluid in the tube	ρ_f^t	10^3 kg m^3
	μ^t	4×10^{-3} kg m s
Fluid in the annulus	ρ_f^a	10^3 kg m^3
	μ^a	10^{-3} kg m s
Viscoelastic solid	ρ_s	10^3 kg m^3
	G	$7{\cdot}85\frac{1+00053\ i\omega}{1+00021\ i\omega} \times 10^3$ Pa

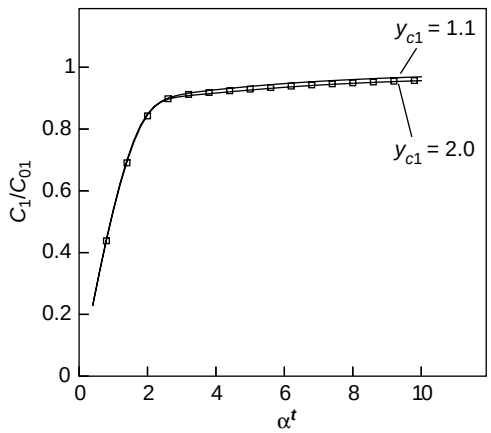

Figure 6. Phase velocity in terms of the Womersley number α^t, for Model 2 and the values of parameters given in Table 2. The phase velocity is normalized with respect to $c_{01} = (E\delta/2\rho_f^t)^{1/2}$. The solid lines show the solutions given by the model for two values of y_{c1}, and the symbols show Womersley's solution. The results are tabulated in Table 3.

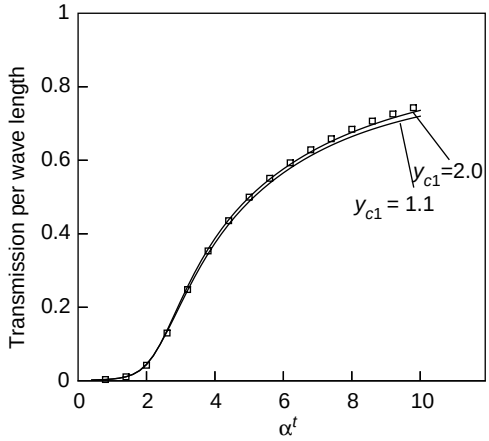

Figure 7. Transmission per wavelength in terms of the Womersley number α^t, for Model 2 and the values of parameters given in Table 2. The solid lines show the solutions given by the model for two values of y_{c1}, and the symbols show Womersley's solution. The results are tabulated in Table 3.

TABLE 3

Phase velocity and transmission per wavelength for Model 2 and the values of parameters given in Table 2, and Womersley's solution for the same values of α^t

			c_1/c_{01}	Trans. per λ
	Womersley		0·22789	0·002203
$\alpha^t = 0{\cdot}4$	Model 2	$y_{c1} = 2{\cdot}0$	0·22887	0·002201
		$y_{c1} = 1{\cdot}1$	0·23076	0·002203
	Womersley		0·84259	0·04238
$\alpha^t = 2{\cdot}0$	Model 2	$y_{c1} = 2{\cdot}0$	0·84626	0·04382
		$y_{c1} = 1{\cdot}1$	0·84915	0·04508
	Womersley		0·95769	0·74827
$\alpha^t = 10{\cdot}0$	Model 2	$y_{c1} = 2{\cdot}0$	0·95668	0·73572
		$y_{c1} = 1{\cdot}1$	0·96915	0·71989

viscoelastic solid with the Maxwell solid or increasing the shear modulus by an order of magnitude has no significant effect on the results, for this value of y_{c1}. In fact, the results differ very little from those obtained for Model 1 and viscous fluids. When $y_{c1} = 1{\cdot}1$, there is a slight increase in the wave speed and in the attenuation for larger α^t. However, the effect is still relatively weak.

Again, we can express all of the constants in terms of A^t and calculate fluid and solid velocities in terms of the driving pressure in the vessel. Table 4 gives area-averaged velocities and flow rates for $\alpha^t = 2$. The solid and the fluid layers between the solid and the rigid tubes both move much slower than either the fluid in the vessel or the fluid between the vessel and the solid. However, due to the large cross-sectional area the volume flux of the solid is significant. The numerical summation of the flow rates confirms that the conservation of volume in the system is satisfied.

TABLE 4

Average velocities and flow rates for different layers in Model 2 calculated for the values of parameters given in Table 2 ($y_{c1} = 2{\cdot}0$), and for $\alpha^t = 2{\cdot}0$

	$(A^t/\rho_f^t c)^{-1} \int \bar{v}_z y \, dy / \int y \, dy$	$2(A^t/\rho_f^t c)^{-1} \int \bar{v}_z y \, dy$	Phase angle
Blood ($0 \leqslant y \leqslant 1$)	0·4643	0·4643	61°
CSF ($1 \leqslant y \leqslant y_{c1}$)	0·0187	0·0561	61°
Tissue ($y_{c1} \leqslant y \leqslant y_{c2}$)	0·0060	0·3607	−124°
CSF ($y_{c2} \leqslant y \leqslant y_0$)	0·0049	0·1764	−107°

4. DISCUSSION

The models show that the main effect of the constraint is to decrease the wave speed for Young's mode, primarily through the action of the normal stresses on the outer surface of the vessel. The magnitude of the normal stress in the annulus is dictated by the conservation of volume in the system. This is evident from the results for Model 1 and inviscid fluids, where the action of the normal stresses on the vessel can be interpreted as an increase of the effective radial inertia of the vessel. The effect of the constraint weakens rapidly with increasing y_0 since the cross-sectional area of the annulus becomes large compared to that of the tube, and a small pressure gradient is sufficient to create a volume flux of the same magnitude as that in the tube. When the medium in the annulus is viscous, the effect of the continuum surrounding the vessel is not eliminated, even when the transverse dimension of the system is infinite (Dinar 1975). However, the results for both Models 1 and 2 with $y_{c1} = 2{\cdot}0$ differ very little from Womersley's solution. We attribute this to the fact that the viscosity of the CSF layer separating the vessel from the tissue is relatively low. When y_{c1} is very small, the effect of the tissue viscosity is more evident.

The analysis is based on the assumption that the amplitudes are small and that the nonlinear terms in the equations of motion can be neglected. The convective term in the Navier–Stokes equations is small compared to the other terms, and the amplitude of the radial vessel motion is much smaller than the R used if $|v_z/c| \ll 1$ (Pedley 1980). In general, these conditions are satisfied for pulse propagation in the arteries outside of the craniospinal cavity. For the model, the condition that the fluid velocity is much smaller than the wave speed has to be satisfied both for the fluid in the tube and the fluid in the annulus. Also, the amplitude of the vessel motion should be much smaller than the width of the annulus. For a large y_0, both of these conditions are satisfied since the fluid velocities in the annulus are small compared to those in the vessel, and the width of the annulus is larger than the tube radius. For $y_0 < 2$ the width of the annulus is smaller than the vessel radius, and for $y_0 < \sqrt{2}$ the average axial velocity in the annulus is larger than that in the vessel. Also, for $y_0 < 2$ the wave speed is considerably reduced due to the constraint. Therefore, the validity of the linear analysis may be questionable for small y_0. However, for physiological applications we are primarily interested in situations where $y_0 > 2$ and the linear analysis should hold.

Much of the analysis was performed using a long wave approximation, which requires that the transverse dimensions of the system be significantly smaller than the wavelength. In our case the long wave approximation is acceptable if κy_0 is small, i.e., the radius of the rigid tube is much smaller than the wavelength. For the larger arteries, the wavelength of

the blood pulse is of the order of a metre, and it increases further down the arterial tree, whereas the dimensions of the cranium and the spinal canal are of the order of 10^{-1} and 10^{-2} m, respectively. Therefore, the long wave approximation should be valid for the range of parameters of interest. The simulations show that the condition for the effect of the constraint to be weak is that y_0 is large, even though κy_0 may still be much smaller than unity. In fact, the effect of the constraint can be very small even if the radius of the rigid tube is of the same order of magnitude as the radius of the vessel.

The model captures the conservation of volume, characteristic of the cranial blood flow, within the framework of a classical linear analysis of pulse propagation in the arteries. Difficulties do arise in the choice of parameters, such as the thickness of the perivascular space. Fortunately, our simulations showed that the solution is affected only if it is assumed that the perivascular space is an order of magnitude smaller than the vessel radius. The model shows: (i) that the speed at which a disturbance propagates in the CSF layer is the same as the speed of blood pulse propagation; (ii) that the CSF pulse is a consequence of volume conservation in the system. A crude estimate of the CSF pulse amplitude made by using equation (29), and $y_0 = 4$ based on the total volumes of blood, CSF, and nervous tissue in the cranium, suggests that the CSF pulse should be an order of magnitude lower than that of the blood pulse. This is within the range of the results reported in the literature (Greenfield and Tindall 1965). Equation (28) can be used in a similar way to relate the movement of the CSF in the spinal cavity with the propagation of the blood pulse. However, in a real physiological system, the CSF pulse reflects the sum of the blood pulses in the craniospinal cavity, and a more thorough insight into the CSF dynamics requires a model that will take into account the whole intracranial network of vessels rather than a single vessel.

5. CONCLUSIONS

The main effect of the constraint imposed on an elastic fluid-filled tube by a coaxial rigid tube filled with incompressible continua is to reduce the wave speed for Young's mode of propagation. The main reason is the increase of the effective radial inertia due to the normal stresses in the fluid in the annulus, necessary to maintain the constant volume in the system. The long wave approximation is justified for the physiologically plausible range of parameters. For Model 1 a closed-form solution is available, whereas for Model 2 an iterative method has to be used.

The principal physiological application of the results is that the dimensions of the skull and the vertebral canal, compared to that of a typical blood vessel, should be large enough to make the effect of the constraint weak. Therefore, we believe that it is appropriate to ignore the effects of the constraint when considering the speed of pulse propagation in the craniospinal cavity. On the other hand, the effect of the constraint is important for the understanding of the CSF pressure pulse and motion, which should be a direct consequence of the blood–CSF coupling necessary to satisfy the conservation of the cranial volume.

ACKNOWLEDGEMENTS

This work has been generously supported by the Canadian Department of National Defence.

References

Atabek, H. B. 1968 Wave propagation through a viscous fluid contained in a tethered, initially stressed, orthotropic elastic tube. *Biophysical Journal* **8,** 626–649.

Atabek, H. B. & Lew, H. S. 1966 Wave propagation through a viscous incompressible fluid contained in an initially stressed elastic tube. *Biophysical Journal* **6,** 481–503.

Cox, R. H. 1968 Wave propagation through a Newtonian fluid contained within a thick-walled, viscoelastic tube. *Biophysical Journal* **8,** 691–709.

Cox, R. H. 1969 Comparison of linearized wave propagation models for arterial blood flow analysis. *Journal of Biomechanics* **2,** 251–265.

Dinar, U. 1975 The role of the surrounding tissue in the propagation of waves through the arterial system. *T. I. T. Journal of Life Sciences* **5,** 49–56.

Dommisse, G. F. 1975 *The Arteries and Veins of the Human Spinal Cord from Birth*. New York, NY: Churchill Livingstone.

Fallenstein, G. T., Hulce, V. D. & Melvin, J. W. 1969 Dynamic mechanical properties of human brain tissue. *Journal of Biomechanics* **2,** 217–226.

Galford, J. E. & McElhaney, J. H. 1970 A viscoelastic study of scalp, brain, and dura. *Journal of Biomechanics* **3,** 211–221.

Gluhbegovic, N. & Williams, T. H. 1980 *The Human Brain: a Photographic Guide*. New York: Harper & Row.

Graff, K. F. 1991 *Wave Motion in Elastic Solids*. New York: Dover.

Gray, F. R. S. 1948 Neurology. In *Anatomy of the Human Body* (ed. M. C. Goss), pp. 737–1019. Philadelphia, PA: Lea & Febiger.

Greenfield, J. C. & Tindall, G. T. 1965 Effect of acute increase in intracranial pressure on blood flow in internal carotid artery of man. *Journal of Clinical Investigation* **44,** 1343–1351.

Guyton, A. C. & Hall, J. E. 1996 *Textbook of Medical Physiology*. London: W. B. Saunders Company.

Hillen, B., Drinkenburg, B. A. H., Hoogstraten, H. W. & Post, L. 1986 Analysis of flow and vascular resistance in a model of the circle of Willis. *Journal of Biomechanics* **21,** 807–814.

Kety, S. S., Shenkin, H. A. & Shmidt, C. F. 1947 The effect of increased intracranial pressure on cerebral circulatory function in man. *Journal of Clinical Investigation* **27,** 493–499.

Lakin, W. D. & Gross, C. E. 1992 A non-linear hemodynamic model for the arterial pulsatile component of the intracranial pulse wave. *Neurological Research* **14,** 219–225.

Lamb, H. 1898 On the velocity of sound in a tube, as affected by the elasticity of the walls. *Manchester Literary and Philosophical Society Memoirs and Proceedings* **42,** 1–16.

Lang, J. 1993 *Clinical Anatomy of the Cervical Spine*. New York: Thieme Medical Publishers Inc.

Ling, S. C. & Atabek, H. B. 1972 A nonlinear analysis of pulsatile flow in arteries. *Journal of Fluid Mechanics* **55,** 493–511.

Loth, F., Yardimci, A. M., Alperin, N. 2001 Hydrodynamic modeling of cerebrospinal fluid motion within the spinal cavity. *Journal of Biomechanical Engineering* **123,** 71–79, doi: 10.1115/1.1336144.

Love, E. A. H. 1944 *A Treatise on the Mathematical Theory of Elasticity*. New York: Dover Publications.

Morgan, G. W. & Kiely, J. P. 1954 Wave propagation in a viscous liquid contained in a flexible tube. *The Journal of the Acoustical Society of America* **26,** 323–328.

Pedley, T. J. 1980 *The Fluid Mechanics of Large Blood Vessels*. Cambridge: Cambridge University Press.

Portnoy, H. D. & Chopp, M. 1994 Intracranial fluid dynamics. *Pediatric Neurosurgery* **20,** 92–98.

Ruan, J. S., Khalil, T. & King, A. I. 1991 Human head dynamic response to side impact by finite element modeling. *Journal of Biomechanical Engineering* **113,** 276–282.

Sheng, C., Sarwal, S. N., Watts, K. C. & Marble, A. E. 1995 Computational simulation of blood flow in human systemic circulation incorporating an external force field. *Medical & Biological Engineering & Computing* **33,** 8–17.

Shuck, L. Z. & Advani, S. H. 1972 Rheological response of human brain tissue in shear. *ASME Journal of Basic Engineering* **94,** 905–911.

Sullivan, H. G. & Allison, J. D. 1985 Physiology of cerebrospinal fluid. In *Neurosurgery* (eds R. Wilkins & S. Rengachary), pp. 2125–2135. New York: McGraw Hill.

TAKEMAE, T. KOSUGI, Y., IKEBE, J., KUMANGI, Y., MATSUYAMA, K. & SAITO, K. 1987 A simulation study of intracranial pressure increment using an electric circuit model of cerebral circulation. *IEEE Transactions on Biomedical Engineering* **34,** 958–962.

URSINO, M. 1988 A mathematical study of human intracranial hydrodynamics part 1—the cerebrospinal fluid pulse pressure. *Annals of Biomedical Engineering* **16,** 379–401.

WANG, D. M. & TARBELL, J. M. 1992 Nonlinear analysis of flow in an elastic tube (artery): steady streaming effects. *Journal of Fluid Mechanics* **239,** 341–358.

WISMAN, J. & VAN OORSCHOT, H. 1993 Omni-directional human head–neck response. In *Biomechanics of Impact Injury and Injury Tolerances of the Head–Neck Complex* (ed. S. H. Backaitis), pp. 193–205. Society of Automotive Engineers.

WOMERSLEY, J. R. 1955 Oscillatory motion of a viscous liquid in a thin-walled elastic tube—I: the linear approximation for long waves. *Philosophical Magazine* **46,** 199–219.

WOMERSLEY, J. R. 1957*a* An elastic theory of pulse transmission and oscillatory flow in mammalian arteries. Technical Report TR 56-614, Wright Air Development Center, Dayton, Ohio, U.S.A.

WOMERSLEY, J. R. 1957*b* Oscillatory flow in arteries: the constrained elastic tube as a model of arterial flow and pulse transmission. *Physics in Medicine and Biology* **2,** 178–187.

WYLIE, C. R. & BARRETT, L. C. 1982 *Advanced Engineering Mathematics*. New York: McGraw-Hill.

ZAGZOULE, M. & MARC-VERGNES, J. P. 1986 A global mathematical model of the cerebral circulation in man. *Journal of Biomechanics* **19,** 1015–1022.

APPENDIX: A

Long Wave Solution for Model 1 and Viscous Fluids

In the long wave approximation, all of the terms of the order κ^2 and $(\kappa/\alpha)^2$ compared with the leading terms are neglected. Also, the asymptotic expressions given in equations (17) are used for the Bessel functions with argument κy. Upon applying the symmetry condition at $y = 0$, constants D_f'' and A_f'' in equations (12) can be eliminated, and the velocities and stresses in the fluid occupying the vessel can be written as

$$\bar{v}_z^t = \frac{\mathrm{J}_0(\alpha^t \mathrm{i}^{3/2} y)}{\mathrm{J}_0(\alpha^t \mathrm{i}^{3/2})} C^t + \frac{A^t}{\rho_f^t c}, \qquad \bar{v}_r^t = \frac{\kappa}{2}\left[\frac{2\mathrm{J}_1(\alpha^t \mathrm{i}^{3/2} y)}{\alpha^t \mathrm{i}^{3/2} \mathrm{J}_0(\alpha^t \mathrm{i}^{3/2})} C^t + \frac{A^t}{\rho_f^t c} y\right],$$
$$\bar{\sigma}_{rz}^t = \rho_f^t c \frac{\kappa}{2} \frac{2\mathrm{J}_1(\alpha^t \mathrm{i}^{3/2} y)}{\alpha^t \mathrm{i}^{3/2} \mathrm{J}_0(\alpha^t \mathrm{i}^{3/2})} C^t, \qquad \bar{\sigma}_{rr}^t = \bar{p}^t = A^t, \tag{A1}$$

where

$$A^t = A_f'^t, \qquad C^t = D_f'^t \mathrm{J}_0(\alpha^t \mathrm{i}^{3/2}), \tag{A2}$$

(Womersley 1957*b*). Upon applying the kinematic conditions at $y = y_0$, constants D_f'' and A_f'' in equations (12) can be expressed in terms of D_f' and A_f', and the fluid velocities and stresses in the annulus can be written as

$$\bar{v}_z^a = \left[\frac{\mathrm{Y}_0(\alpha^a \mathrm{i}^{3/2} y_0)\mathrm{J}_0(\alpha^a \mathrm{i}^{3/2} y) - \mathrm{J}_0(\alpha^a \mathrm{i}^{3/2} y_0)\mathrm{Y}_0(\alpha^a \mathrm{i}^{3/2} y)}{\mathrm{Y}_0(\alpha^a \mathrm{i}^{3/2} y_0)\mathrm{J}_0(\alpha^a \mathrm{i}^{3/2}) - \mathrm{J}_0(\alpha^a \mathrm{i}^{3/2} y_0)\mathrm{Y}_0(\alpha^a \mathrm{i}^{3/2})}\right] C^a$$

$$+ \left[1 - \frac{\mathrm{Y}_0(\alpha^a \mathrm{i}^{3/2} y)}{\mathrm{Y}_0(\alpha^a \mathrm{i}^{3/2} y_0)}\right] \frac{A^a}{\rho_f^a c},$$

$$\bar{v}_r^a = \left(\frac{\kappa}{2}\right)\left\{\left[\frac{2(\mathrm{Y}_0(\alpha^a \mathrm{i}^{3/2} y_0)\mathrm{J}_1(\alpha^a \mathrm{i}^{3/2} y_0) - \mathrm{J}_0(\alpha^a \mathrm{i}^{3/2} y_0)\mathrm{Y}_1(\alpha^a \mathrm{i}^{3/2} y))}{\alpha^a \mathrm{i}^{3/2}(\mathrm{Y}_0(\alpha^a \mathrm{i}^{3/2} y_0)\mathrm{J}_0(\alpha^a \mathrm{i}^{3/2}) - \mathrm{J}_0(\alpha^a \mathrm{i}^{3/2} y_0)\mathrm{Y}_0(\alpha^a \mathrm{i}^{3/2}))}\right.\right.$$

$$\left.\left. - \left(\frac{y_0}{y}\right)\frac{2(\mathrm{Y}_0(\alpha^a \mathrm{i}^{3/2} y_0)\mathrm{J}_1(\alpha^a \mathrm{i}^{3/2} y_0) - \mathrm{J}_0(\alpha^a \mathrm{i}^{3/2} y_0)\mathrm{Y}_1(\alpha^a \mathrm{i}^{3/2} y_0))}{\alpha^a \mathrm{i}^{3/2}(\mathrm{Y}_0(\alpha^a \mathrm{i}^{3/2} y_0)\mathrm{J}_0(\alpha^a \mathrm{i}^{3/2}) - \mathrm{J}_0(\alpha^a \mathrm{i}^{3/2} y_0)\mathrm{Y}_0(\alpha^a \mathrm{i}^{3/2}))}\right] C^a\right.$$

$$\left. + \left[\left(y - \frac{2\mathrm{Y}_1(\alpha^a \mathrm{i}^{3/2} y)}{\alpha^a \mathrm{i}^{3/2}\mathrm{Y}_0(\alpha^a \mathrm{i}^{3/2} y_0)}\right) - \left(\frac{y_0}{y}\right)\left(y_0 - \frac{2\mathrm{Y}_1(\alpha^a \mathrm{i}^{3/2} y_0)}{\alpha^a \mathrm{i}^{3/2}\,\mathrm{Y}_0(\alpha^a \mathrm{i}^{3/2} y_0)}\right)\right]\frac{A^a}{\rho_f^a c}\right\}, \tag{A3}$$

$$\bar{\sigma}_{rz}^a = \rho_f^a c\,\frac{\kappa}{2}\left\{\left[\frac{2(\mathrm{Y}_0(\alpha^a \mathrm{i}^{3/2} y_0)\mathrm{J}_1(\alpha^a \mathrm{i}^{3/2} y) - \mathrm{J}_0(\alpha^a \mathrm{i}^{3/2} y_0)\mathrm{Y}_1(\alpha^a \mathrm{i}^{3/2} y))}{\alpha^a \mathrm{i}^{3/2}(\mathrm{Y}_0(\alpha^a \mathrm{i}^{3/2} y_0)\mathrm{J}_0(\alpha^a \mathrm{i}^{3/2}) - \mathrm{J}_0(\alpha^a \mathrm{i}^{3/2} y_0)\mathrm{Y}_0(\alpha^a \mathrm{i}^{3/2}))}\right] C^a\right.$$

$$\left. - \frac{2\mathrm{Y}_1(\alpha^a \mathrm{i}^{3/2}\, y)}{\alpha^a \mathrm{i}^{3/2}\mathrm{Y}_0(\alpha^a \mathrm{i}^{3/2} y_0)}\frac{A^a}{\rho_f^a c}\right\}, \quad \bar{\sigma}_{rr}^a = \bar{p}^a = A^a,$$

where the new constants A^a and C^a are defined as

$$A^a = A_f'^a,$$

$$C^a = \frac{\mathrm{Y}_0(\alpha^a \mathrm{i}^{3/2} y_0)\mathrm{J}_0(\alpha^a \mathrm{i}^{3/2}) - \mathrm{J}_0(\alpha^a \mathrm{i}^{3/2} y_0)\mathrm{Y}_0(\alpha^a \mathrm{i}^{3/2})}{\mathrm{Y}_0(\alpha^a \mathrm{i}^{3/2} y_0)} D_f'^a. \tag{A4}$$

When the kinematic conditions are applied at the vessel wall, constants C^t, A^t, C^a and A^a can be expressed in terms of M and N, and the linearized equations of motion of the vessel [equation (16)] can be written as

$$\begin{bmatrix} \delta - X + \frac{1}{2}\Theta_{zz} & \varepsilon X - \Theta_{rz} \\ \varepsilon X - \Theta_{rz} & -X + 2\Theta_{rr} \end{bmatrix} \begin{Bmatrix} \kappa M \\ N \end{Bmatrix} = \begin{Bmatrix} 0 \\ 0 \end{Bmatrix}, \tag{A5}$$

where

$$\Theta_{zz} = \frac{\mathrm{F}_{10}(\alpha^t)}{1 - \mathrm{F}_{10}(\alpha^t)} + \left(\frac{\rho_f^a}{\rho_f^t}\right)$$

$$\frac{\mathscr{F}(1, y_0, \alpha^a)[\mathscr{G}(y_0, y_0, \alpha^a) - 1] - \mathscr{F}(y_0, y_0, \alpha^a)[\mathscr{G}(1, y_0, \alpha^a) - 1]}{[\mathscr{G}(1, y_0, \alpha^a) - \mathscr{G}(y_0, y_0, \alpha^a)] - \mathscr{H}(y_0, \alpha^a)[\mathscr{F}(1, y_0, \alpha^a) - \mathscr{F}(y_0, y_0, \alpha^a)]},$$

$$\Theta_{rz} = \frac{\mathrm{F}_{10}(\alpha^t)}{1 - \mathrm{F}_{10}(\alpha^t)} - \left(\frac{\rho_f^a}{\rho_f^t}\right)$$

$$\frac{[\mathscr{F}(1, y_0, \alpha^a) - \mathscr{F}(y_0, y_0, \alpha^a)]}{[\mathscr{G}(1, y_0, \alpha^a) - \mathscr{G}(y_0, y_0, \alpha^a)] - \mathscr{H}(y_0, \alpha^a)[\mathscr{F}(1, y_0, \alpha^a) - \mathscr{F}(y_0, y_0, \alpha^a)]},$$

$$\Theta_{rr} = \frac{1}{1 - \mathrm{F}_{10}(\alpha^t)} - \left(\frac{\rho_f^a}{\rho_f^t}\right)$$

$$\frac{1}{[\mathscr{G}(1, y_0, \alpha^a) - \mathscr{G}(y_0, y_0, \alpha^a)] - \mathscr{H}(y_0, \alpha^a)[\mathscr{F}(1, y_0, \alpha^a) - \mathscr{F}(y_0, y_0, \alpha^a)]}, \tag{A6}$$

function F_{10} is given by

$$F_{10}(\alpha) = \frac{2J_1(\alpha i^{3/2})}{\alpha i^{3/2} J_0(\alpha i^{3/2})} \tag{A7}$$

(Womersley 1957*b*), and functions $\mathscr{F}$, $\mathscr{G}$, and $\mathscr{H}$ are defined as

$$\mathscr{F}(x, y_0, \alpha) = \frac{2x[Y_0(\alpha i^{3/2} y_0) J_1(\alpha i^{3/2} x) - J_0(\alpha i^{3/2} y_0) Y_1(\alpha i^{3/2} x)]}{\alpha i^{3/2}[Y_0(\alpha i^{3/2} y_0) J_0(\alpha i^{3/2}) - J_0(\alpha i^{3/2} y_0) Y_0(\alpha i^{3/2})]},$$

$$\mathscr{G}(x, y_0, \alpha) = x^2 - \frac{2x Y_1(\alpha i^{3/2} x)}{\alpha i^{3/2} Y_0(\alpha i^{3/2} y_0)}, \tag{A8}$$

$$\mathscr{H}(y_0, \alpha) = 1 - \frac{Y_0(\alpha i^{3/2})}{Y_0(\alpha i^{3/2} y_0)}.$$

The first term on the right-hand side of equations (A6) corresponds to Womersley's solution for an unconstrained tube, whereas the second term accounts for the effect of the constraint.